ORIGINAL RESEARCH ARTICLE

Spatio-temporal variability of the phytoplankton biomass in the Levantine basin between 2002 and 2015 using MODIS products

Roy El Hourany [a], Ali Fadel [a], Elissar Gemayel [b], Marie Abboud-Abi Saab [b], Ghaleb Faour [a],*

[a] *National Center for Remote Sensing, National Council for Scientific Research (CNRS), Beirut, Lebanon*
[b] *National Center for Marine Sciences, National Council for Scientific Research (CNRS), Batroun, Lebanon*

Summary   The Levantine basin in the Eastern Mediterranean Sea is subject to spatial and seasonal variations in primary production and physical-chemical properties both on a short and long-term basis. In this study, the monthly means of daily MODIS product images were averaged between 2002 and 2015, and used to characterize the phytoplankton blooms in different bioregions of the Levantine basin. The selected products were the sea surface temperature (SST), the chlorophyll-*a* concentration (Chl-*a*), the diffuse attenuation coefficient for down-welling irradiance at 490 nm (Kd_490) and the colored dissolved organic matter index (CDO-M_index). Our results showed that phytoplankton blooms were spatially and temporally variable. They occurred in late autumn at the Nile Delta, in early spring and late summer at the eastern coastline, and in spring at the northeastern coastline. The northern coastline and the open water had a common bloom occurring in winter. The Nile Delta was found to be the most productive area of the Levantine basin showing high Chl-*a*. Kd_490 and Chl-*a* present a parallel co-variation indicating a dominance of Case 1 waters in the Levantine basin. The CDOM_index shows a phase shift with the Chl-*a* fluctuation. A strong inverse correlation was observed between both Chl-*a* and CDOM_index with SST, connoting an indirect relation represented by a depression of CDOM in summer by photobleaching, and a suppression of the chlorophyll-*a* concentration due to water

---

* Corresponding author at: National Center for Remote Sensing, National Council for Scientific Research (CNRS), P.O. Box 11-8281, Riad El Solh, 1107 2260 Beirut, Lebanon. Tel.: +961 3823423.
    E-mail address: gfaour@cnrs.edu.lb (G. Faour).

stratification, together with nutrient stress. An overestimation of the Chl-*a* values had been signaled by the use of the CDOM_index, suggesting a correction plan in a latter study.

1. Introduction

The Mediterranean Sea is a semi-enclosed basin, covering approximately 0.8% of the world's ocean surface area. Although it has limited geographical dimensions, it is considered one of the most complex marine environments where little is known with regard to circulation dynamics, biogeochemistry and biological activity (Tanhua et al., 2013). The Mediterranean Sea presents a deficit in hydrological balance, as evaporation exceeds the supply of fresh water from streams and precipitation. This deficit is partially compensated by the inflow of Atlantic waters through the Strait of Gibraltar. This results in fresh, nutrient-poor surface flow into the basin with saltier, nutrient-richer deeper water outflow through the Strait of Gibraltar (Bethoux et al., 1992). Hydrological differences along the basin cause the presence of an increasing oligotrophic gradient from west to east.

The Eastern Mediterranean behaves in a similar manner, with surface inflow and deeper water outflow through the Straits of Sicily. This results in a west to east gradient of decreasing surface chlorophyll-*a* concentration (Chl-*a*) (Turley et al., 2000) that was observed from space (Antoine et al., 1995), with the Eastern Mediterranean Levantine waters exhibiting highly oligotrophic conditions. As a result, surface Chl-*a* in the Levantine basin normally don't exceed 0.4 mg m^{-3} (Abdel-Moati, 1990; Dowidar, 1984; Krom et al., 1991; Yacobi et al., 1995) except near the Nile Delta coast and other adjacent coasts where it can reach up to 80 mg m^{-3} (EIMP-CWMP, 2007).

The Levantine basin regroups the Egyptian northern coast where the Nile River discharges on its delta, the Sinai Peninsula's northern coast, the Israeli coast, the Lebanese coast, the Syrian coast, the southern Turkish coast and the coast of Cyprus. This region is nourished by small water streams, and the Nile River.

The knowledge of the space and time heterogeneity of phytoplankton growth in oligotrophic to ultra-oligotrophic conditions is essential to understand the marine ecosystem dynamics (Mann and Lazier, 2006). In the last decade, remote sensing of surface optical properties has provided synoptic views of the abundance and distribution of sea surface constituents, such as the concentration of Chl-*a* pigments (Su et al., 2015). Nowadays, many studies showed that time series of remotely sensed data can provide information on phytoplankton growth patterns, and related environmental conditions, to serve *in situ* assessments of ecosystem dynamics over wide space and time scales (Brando et al., 2012; Devlin et al., 2012; Kennedy et al., 2012; Schroeder et al., 2012).

The aim of the present work is to assess recurrent algal blooms in the Levantine basin, by using optical remote sensing data. To this end, a time series of data collected by the MODIS Terra and Aqua missions was selected to explore the large-scale, long-term features of the Chl-*a* fields in the Levantine basin, between 2002 and 2015. In the following the MODIS-derived multi-annual database, used here to examine the variability of the Chl-*a* field at a monthly and climatological scale, will be introduced, together with a statistical application. Finally, the spatiotemporal patterns emerging from this analysis will be discussed, simultaneously with other MODIS remotely sensed parameters; sea surface temperature (SST), colored dissolved organic matter index (CDOM_index), and the diffuse attenuation coefficient for downwelling irradiance at 490 nm (Kd_490) and compared to previous studies results.

2. Material and methods

The MODIS Terra and aqua daily Level 2 products of SST, Chl-*a*, CDOM_index and Kd_490 computed with sensor standard algorithms from 2002 till 2015 were provided by the oceancolor.gsfc.nasa.gov portal.

The standard OC3 algorithm returns the near-surface Chl-*a* in mg m^{-3} at a spatial resolution of 1 km, calculated using an empirical relationship derived from *in situ* measurements of Chl-*a* and blue-to-green band ratios of water-leaving remote sensing reflectances (Rrs) developed by O'Reilly et al. (1998) and can be expressed as the following:

$$\log_{10}(\text{Chl-}a) = 0.2424 - 2.7423R + 1.8017R^2 + 0.0015R^3 - 0.1228R^4 \quad (1)$$

with

$$R = \log_{10}\left(\frac{\text{Max}(\text{Rrs}_{443}, \text{Rrs}_{488})}{\text{Rrs}_{547}}\right). \quad (2)$$

The empirical algorithm OC3M is an adapted form for MODIS, developed from SeaWiFS OC2 and OC4 algorithms.

Level 2 satellite-to-*in situ* match-up validation results are available for MODIS from the validation tool of the SeaWiFS Bio-Optical Archive and Storage System (SeaBASS), showing a global correlation coefficient above 0.75 with a RMSE = 0.3 mg m^{-3}. For this study, the same standard sensor algorithm was used for waters differing in the degree of eutrophication.

For the SST estimation, the satellite measurement is made by sensing the ocean radiation in two or more wavelengths within the infrared part of the electromagnetic spectrum which can then be empirically related to SST. In this case, the MODIS SST product provides sea surface temperature [°C] at a spatial resolution of 1 km.

The Kd_490 (in m^{-1}, 1-km spatial resolution) is calculated using an empirical relationship derived from *in situ* spectroradiometric data from oceanographic stations of Kd_490 and blue-to-green band ratios of remote sensing reflectances (Rrs) belonging to a wide variety of water types (Austin and Petzold, 1981).

The sensor default algorithm can be expressed as the following:

$$KD2M: \quad \log_{10}(K_{bio}(490)) = -0.8813 - 2.035R + 2.5878R^2$$
$$- 3.4885R^3 - 1.5061R^4, \quad (3)$$

$$Kd_{490} = K_{bio}(490) + 0.0166 \quad (4)$$

with

$$R = \log_{10}\left(\frac{Rrs_{488}}{Rrs_{547}}\right). \quad (5)$$

Examining the consistency of the empirical algorithm has been the object of many studies (Lee, 2005; Morel et al., 2007; O'Reilly et al., 2000; Werdell and Bailey, 2005; Yeh et al., 1997).

And last, Morel and Gentili (2009) stated that the CDOM absorption coefficient, noted α, tends to increase with increasing Chl-a in a non-linear manner, according to:

$$\alpha(400; \text{Chl-}a) = 0.065 \, \text{Chl-}a^{0.63}. \quad (6)$$

A quantitative way of analytically showing the relationship when the CDOM—[Chl] proportions change, consists of imposing deviations from the equation above, by introducing a factor larger or lesser than unity, noted as CDOM_index:

$$\alpha(400; \text{Chl-}a) = \text{CDOM}_{index} 0.065 \, \text{Chl-}a^{0.63}. \quad (7)$$

The α values for the other wavelengths of interest are:

$$\alpha(412; \text{Chl-}a) = \text{CDOM}_{index} 0.0524 \, \text{Chl-}a^{0.63}, \quad (8)$$

$$\alpha(440; \text{Chl-}a) = \text{CDOM}_{index} 0.0316 \, \text{Chl-}a^{0.63}, \quad (9)$$

$$\alpha(490; \text{Chl-}a) = \text{CDOM}_{index} 0.0129 \, \text{Chl-}a^{0.63}, \quad (10)$$

$$\alpha(555; \text{Chl-}a) = \text{CDOM}_{index} 0.004 \, \text{Chl-}a^{0.63}. \quad (11)$$

The colored dissolved organic matter index (Level 2, 1-km resolution) quantifies the deviation in the relationship between the absorption of CDOM and Chl-a, where 1 represents the mean for Case 1 waters, and values above or below 1 indicate excess or deficit in CDOM (Morel and Gentili, 2009). Its primary purpose is to correct chlorophyll retrievals as the index provides a direct estimate of a deviation index, described as the ratio between the actual CDOM content and the normal content, expected in Case 1 waters from the local chlorophyll concentration. Therefore, the index value above or below 1 can indicate an underestimation or overestimation of the estimated Chl-a using the standard sensor algorithm. The only validation work was performed by Morel and Gentili (2009) following the algorithm retrieval.

A selection of 4173 daily images was performed for each product while merging both MODIS Terra and Aqua daily images in order to select and retain the maximum of best quality pixels. The selection of these pixels was possible due to many quality Level 2 flags and masks suggested on SeaDas, complying with the masks used for the Level 3 binned products on the oceancolor.gsfc.nasa.gov portal. The binning process is based on the NASA SeaWiFS binning operator, giving the ability to aggregate the pixel data into arithmetic mean while confining to each pixel its place in a Level 3 grid using a geographical information system. While calculating the arithmetic mean, the quality flags and masks allow excluding the pixels that are affected by clouds, sunglint, very high radiance, straylight contamination, low water leaving radiance, algorithm failure, atmospheric correction failure and suspected navigation quality. In the end, the output that emerges from this process is a time series of binned monthly images with a resolution of 1 km^2.

3. Information retrieval

Lavender et al. (2009) have conducted a research over the Egyptian continental shelf to assess the temporal shifts of the chlorophyll level in this region and detect the Nile's bloom between 1997 and 2006. In order to detect the surface Chl-a variability and its spatial changes across the Delta shelf, the area was divided geographically into two bio-geographical areas, the inner (0—50 m depth) and outer (50—200 m depth) shelf, based on knowledge of the biophysical regimes (effects alongshore currents and surface run-off on quality and productivity of coastal water off the delta coast).

Therefore, a similar division was applied in this study, on the Nile delta's shelf and on the Gulf of Iskenderun due to the presence of a large continental shelf, while also adding an open water zone (>200 m in depth) as a bio-geographical area. Along the eastern and northern coastlines, an additional bio-geographical area was also created: from 0 till 200 m in depth, regarding the narrowness of the continental shelf and the number of pixels covered by this area (Fig. 1).

In order to determine each subdivision's ocean color characteristics, a bathymetry image (ETOPO-1 bedrock) is used to limit each subdivision in a drawn bathymetry mask using ArcGIS 10. ETOPO1 is an arc-minute global relief model of Earth's surface that integrates land topography and ocean bathymetry. It was built from numerous global and regional data sets and provided by NOAA agency and acquired from ngdc.noaa.gov.

The calculated average of every subdivision for each of the parameters was done using ArcGIS 10 while extracting the value of the pixels averaged under each of the bathymetry mask, and followed by a statistic study performed on SPSS statistics 20. The latter consists on the retrieval of the maxima, minima, average, and standard deviation of the parameters time series for each subdivision. A Pearson correlation study was performed *via* pairing the time series of Chl-a and Kd_490, Chl-a and CDOM_index, Chl-a and SST and finally CDOM_index and SST for each subdivision.

4. Results

4.1. Statistical and climatology results

The biogeographic subdivisions were applied on the computed monthly images of SST (Fig. 2), Chl-a (Fig. 3), CDOM_index (Fig. 4) and Kd_490 (Fig. 5) in order to assess the variation of these features monthly between 2002 and 2015.

The recordings of the sea surface temperature between 2002 and 2015 follow an annual cycle with the lowest temperatures in February and March and the highest temperatures in July and August. In this time laps, the lowest monthly sea surface temperature average recorded was on February
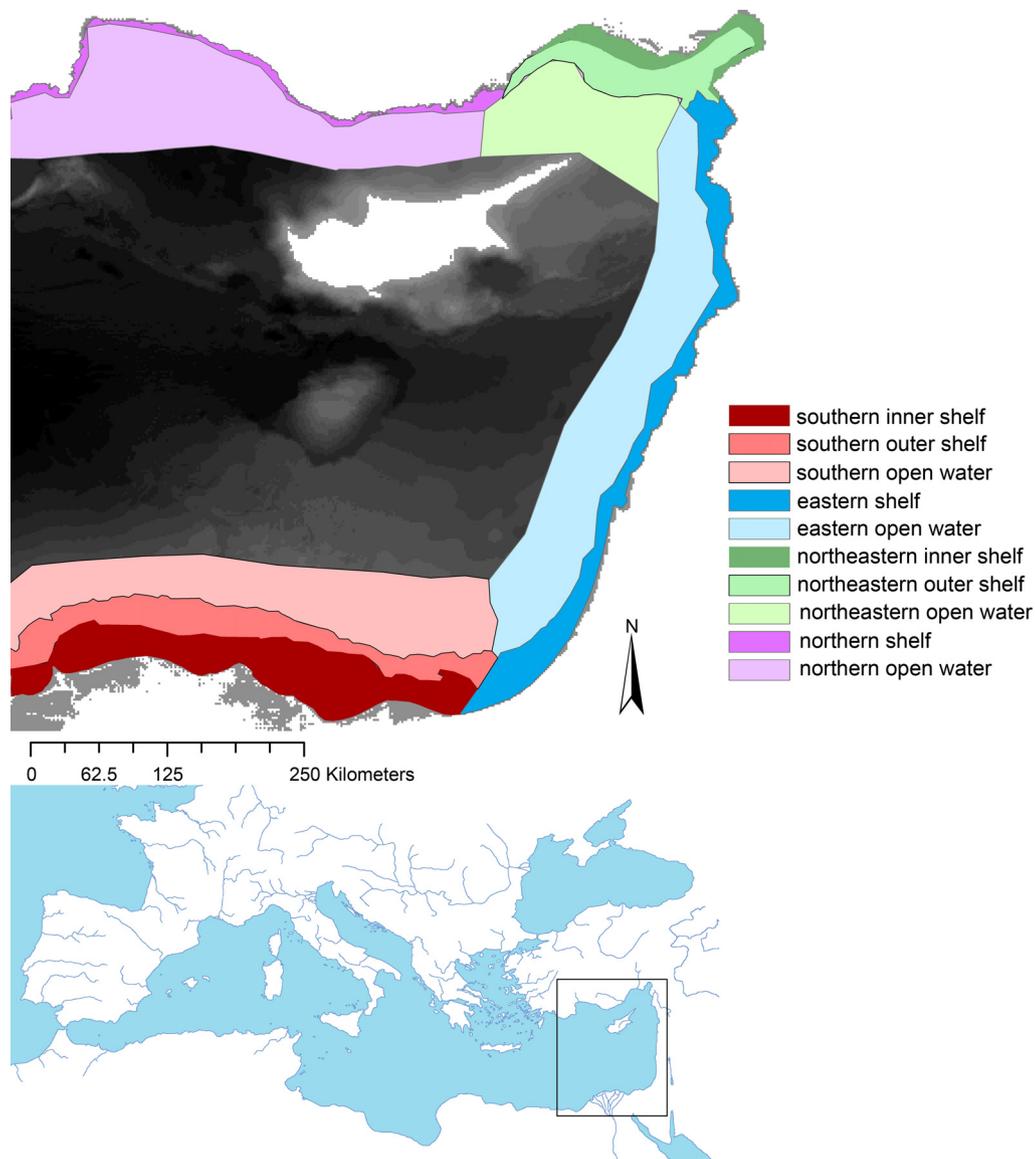
Figure 1 The Levantine basin subdivided into biogeographic regions using ETOPO-1 bathymetry map.

2004 with 16.51°C, and the highest monthly temperature average recorded was on August 2012 with 29.22°C.

The monthly averaged Chl-*a* (Fig. 6) shows a seasonal rhythmicity in open water, but it is altered while moving to the coast, characterized with higher Chl-*a* and turbid waters. These results show that the monthly climatology of Chl-*a* (Fig. 7) is different for each biogeographic subdivision. For instance, the southern coastal region is characterized by an increase of Chl-*a* in late autumn, reaching a maximum mean of 2.8 mg m^{-3} in December 2010, whereas in the eastern coastal region the Chl-*a* peak is observed in late winter, recording a peak of 1.28 mg m^{-3} in April 2006, and early autumn, reaching a maximum mean of 1.1 mg m^{-3} in September 2005. In the Gulf of Iskenderun and Mersin Bay, the Chl-*a* peak is observed in spring, reaching a maximum mean of 3.8 mg m^{-3} in April 2012, followed by a slight increase in late summer, and in the northern coastal region the Chl-*a* reach a maximum in winter, at 1.1 mg m^{-3} in February 2009. Finally, in the open water region, the Chl-*a* peak is observed in winter, reaching a maximum mean at 0.33 mg m^{-3} (Table 1).

The monthly average of the Kd_490 ranges between 0.2 m^{-1} (22.5 m of euphotic depth) in December 2010 and 0.12 m^{-1} in June 2007 near the delta, 0.11 m^{-1} in April 2006 (41 m of euphotic depth) and 0.04 m^{-1} in May 2014 near the eastern coast, 0.27 m^{-1} (16.7 m of euphotic depth) in April 2012 and 0.08 m^{-1} in March 2014 at the Gulf of Iskenderun and Mersin Bay, 0.1 m^{-1} (45 m of euphotic depth) and 0.03 m^{-1} in July 2014 at the northern coast (Table 1).

The CDOM_index values are all above 1, fluctuating between 2 and 5.78. The index shows that the highest overall mean is recorded on the southern inner shelf with 4.25. Yet the correspondent variability within the series from 2002 till 2015 is the least, recording a standard deviation of 0.54. On the other hand, the lowest mean is recorded on the northern shelf, with an index of 3.17, and with the highest correspondent standard deviation of 0.86 within the time series. While observing the CDOM_index climatology images, a preeminent cluster of high CDOM_index is visible at the southern outer shelf and at the northeastern outer shelf and some regions witness a seasonal CDOM_index fluctuation (Table 1).
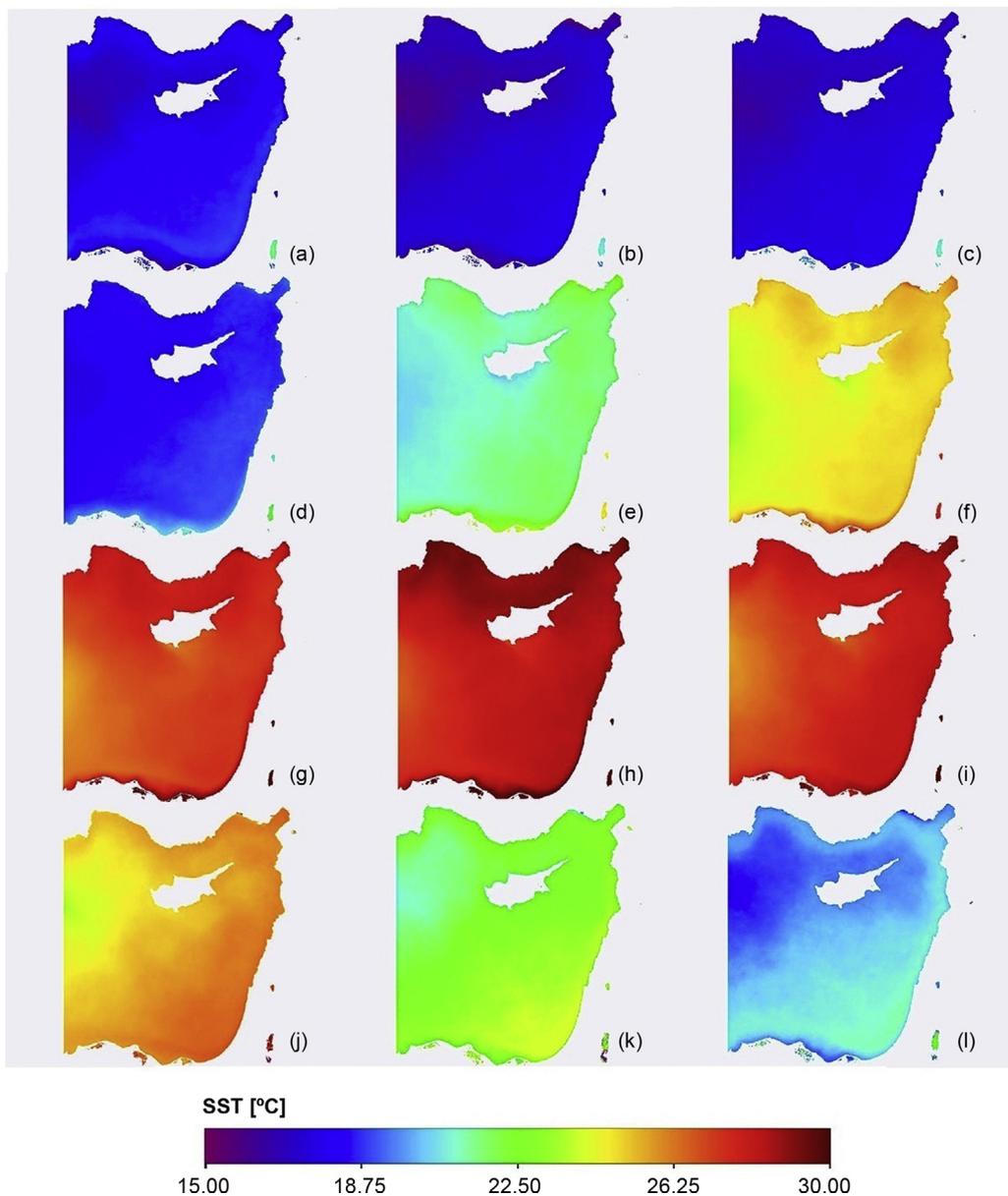
Figure 2 Monthly climatology sea surface temperature averaged using Level 2 SST data from MODIS Aqua and Terra, over the 14 studied years in the Levantine basin [(a) January, (b) February, (c) March, (d) April, (e) May, (f) June, (g) July, (h) August, (i) September, (j) October, (k) November, (l) December].

The climatology monthly average calculated for each parameter for the Levantine basin (Fig. 8) shows that the Chl-*a* and Kd_490 are covariant, drawing a similar behavior recording the highest values in February, and the lowest in July. Whereas the CDOM_index is ahead with a one-month phase shift, showing a maximum index value in March and the lowest value in September. The SST is inversely behaving where the highest SST recorded in August and the lowest in February.

4.2. Pearson correlation results

The correlation between the Chl-*a* and the attenuation coefficient Kd_490 monthly means was highly significant in all biogeographic subdivisions (above 0.9, significant at the 0.01 level) (Fig. 9).

The Chl-*a* and the colored dissolved organic matter index monthly means were weakly correlated in the subdivisions (0; −50 m). However, the correlation strengthens while passing gradually to the open waters, representing a correlation factor shifting from 0.009 and 0.128 at the shelf to a significant 0.57 in the open waters. In addition, the correlative analysis between the two products data (Chl-*a*, CDOM_index) and the SST monthly means showed a high inverse correlation factor while moving far from the coast, noting the passage from 0.157 to a significant 0.759 between SST and Chl-*a*, and from 0.088 to a significant 0.7 between SST and CDOM_index, significant at the 0.01 level (Fig. 9).
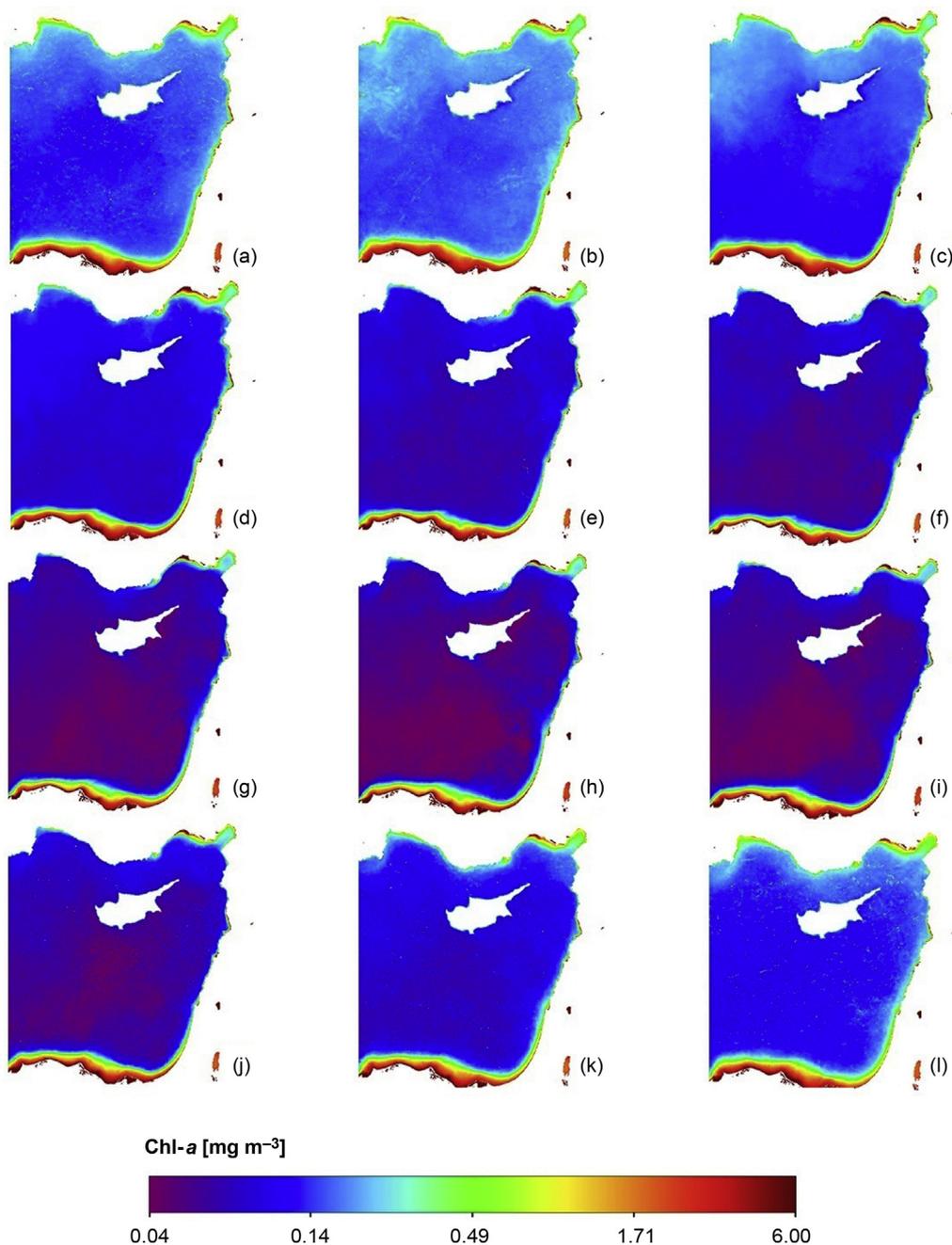
Figure 3   Monthly climatology chlorophyll-*a* concentration averaged using Level 2 Chl-*a* data from MODIS Aqua and Terra, over the 14 studied years in the Levantine basin [(a) January, (b) February, (c) March, (d) April, (e) May, (f) June, (g) July, (h) August, (i) September, (j) October, (k) November, (l) December].

5. Discussion

5.1. Algal bloom patterns

The increase of Chl-*a* is a result of the phytoplankton heavy multiplication inducing seasonal blooms. This occurs when the climatic and biochemical factors are propitious, such as the elevation of the SST, the increase of the sun irradiance budget and the availability of nutrients such as phosphates and nitrates (Krom et al., 2003).

The climatology images of Chl-*a* and the descriptive statistics show that the most productive regions of the Levantine basin are the Nile's Delta, the Gulf of Iskenderun and Mersin bay. This relatively high productivity is due to the higher nutrient inputs (rivers and pollution sources) and the presence of a larger continental shelf where the majority of the oceanic burial of organic carbon occurs (Hedges and Keil, 1995; Premuzic et al., 1982). The Chl-*a* climatology results showed a seasonal cycle at the Nile Shelf, the Chl-*a* starts to arise in autumn to reach a maximum in winter (February). This bloom is accounted to the Nile flood that occurs each early autumn
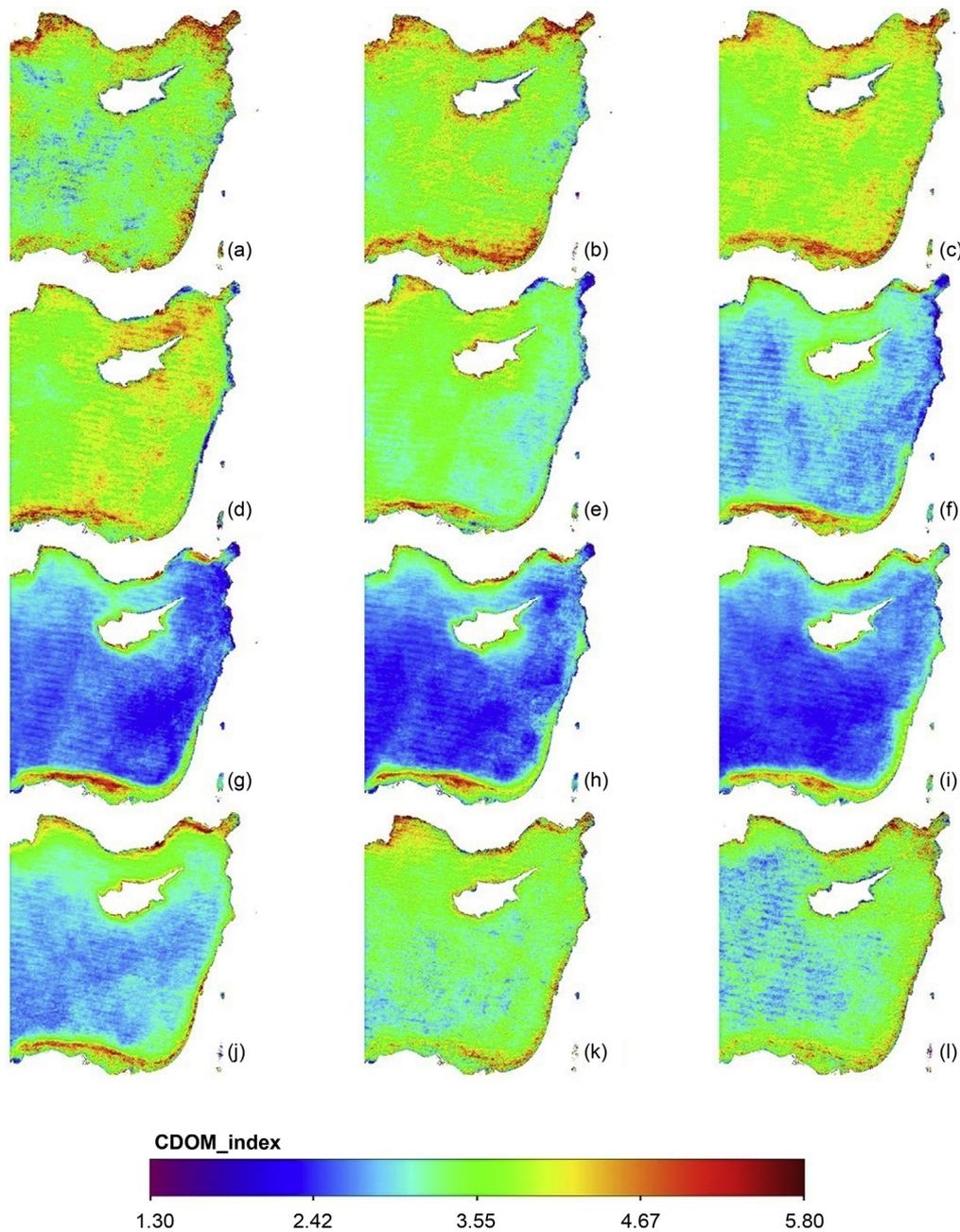
Figure 4   Monthly climatology colored dissolved organic matter index averaged using Level 2 CDOM_index data from MODIS Aqua and Terra, over the 14 studied years in the Levantine basin [(a) January, (b) February, (c) March, (d) April, (e) May, (f) June, (g) July, (h) August, (i) September, (j) October, (k) November, (l) December].

(Lavender et al., 2009). Adding to that, a maximum average of 2.75 mg m^{-3} is noted in February at the Nile delta, which is in agreement with the study of Dowidar (1984) estimating a Chl-a maximum of 2.8 mg m^{-3} observed in winter.

On the other hand, at the northeastern subdivisions where the Gulf of Iskenderun and Mersin bay are located, the Chl-a peaks exponentially indicating an early spring phytoplankton bloom, due to the propitious climatic factors in this season, and decrease gradually and slowly till winter. The slight increase of Chl-a in August suggests the presence of an autumnal bloom. This regime points at the richness of this coastal zone, where the nutrient load is not a limiting factor. The Gulf of Iskenderun and Mersin Bay are both situated in the

south of Turkey and are subjected to heavy anthropogenic activities (Karakaya and Evrendilek, 2011; Yilmaz et al., 1992). The increase in accumulating input of nutrients like nitrogen and phosphorus *via* Ceyhan (Gulf of Iskenderun) and Yenice (Mersin Bay) rivers and man-made run offs promotes phytoplankton and phytobenthos production (Yilmaz et al., 1992).

Meanwhile, the eastern and northern coastline is less productive, compared to both the southern and northeastern areas of the Levantine basin. This may be associated with the presence of a narrow shelf with no prominent upwelling phenomenon (Caddy, 1998) (Fig. 1).

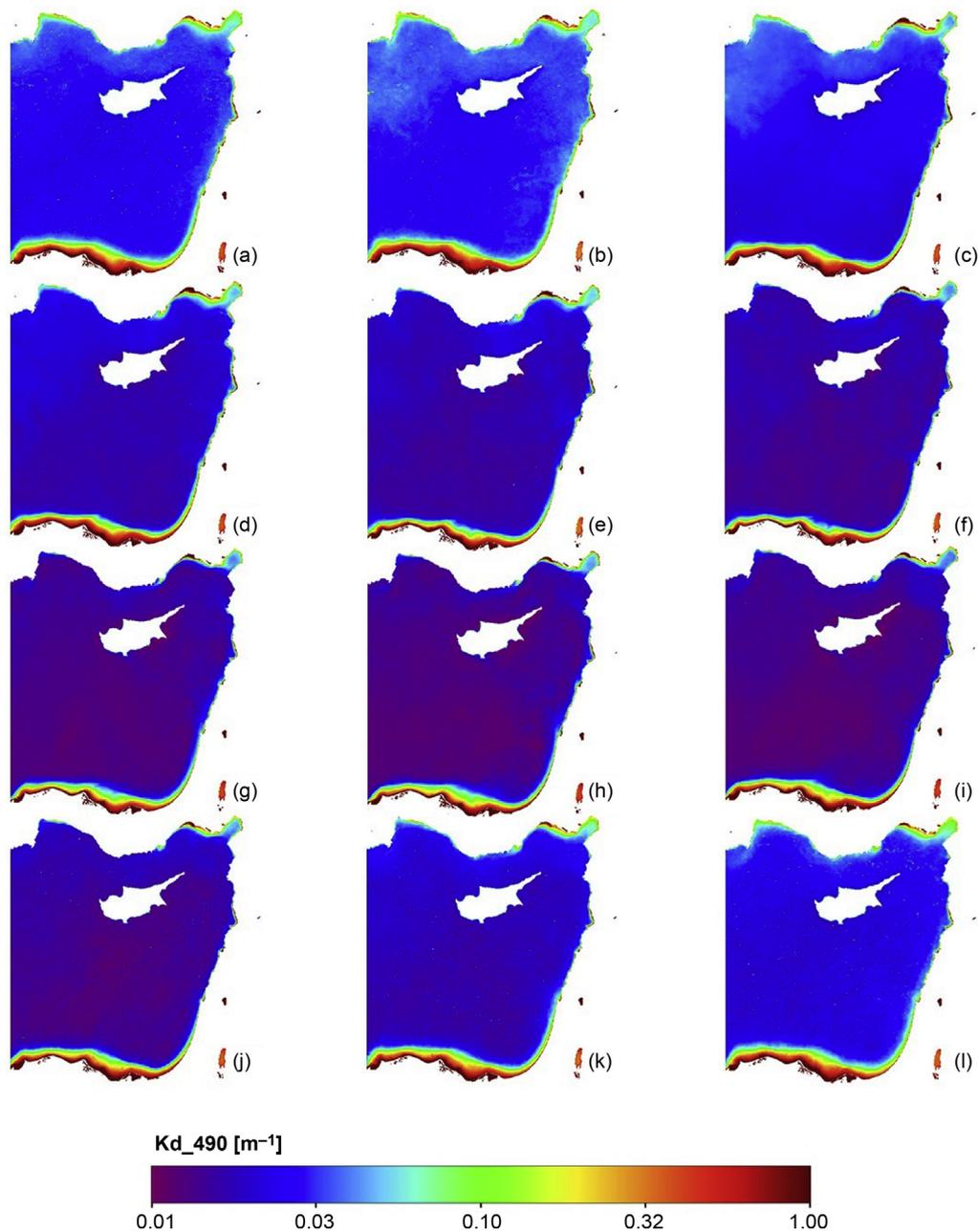In this study two conspicuous phytoplankton blooms were observed at the eastern coastline: a spring bloom in March—

Kd_490 [m⁻¹]

Figure 5   Monthly climatology diffuse attenuation coefficient for downwelling irradiance at 490 nm averaged using Level 2 Kd_490 data from MODIS Aqua and Terra, over the 14 studied years in the Levantine basin [(a) January, (b) February, (c) March, (d) April, (e) May, (f) June, (g) July, (h) August, (i) September, (j) October, (k) November, (l) December].

April and autumnal bloom peaking by the end of August. The autumnal blooms are accounted to the regenerated nutrient stuck in the upper layer of the sea after the settlement of the summer thermocline. The average Chl-a concentrations near the same coastal region ranged between 0.29 and 1.29 mg m⁻³ which is consistent with the results of Abboud-Abi Saab (1992), Abboud-Abi Saab et al. (2008) and Azov (1986) at the eastern coast, where Chl-a ranged between 0.1 and 1 mg m⁻³. Many sites along the coast show higher values of Chl-a and Kd_490 within the climatology images. These sites correspond to major cities and their seaports (Tartous in Syria, Beirut, Jounieh and Sidon in Lebanon, Haifa, Netanya and Tel Aviv in Israel), water stream estuaries and agricultural crops near

the coast (such as Al Hamidiyah in Syria). The combination of these factors induces the fertilization of the coastal waters and leads to an increase of the phytoplankton biomass and the suspended particles abundance.

The northern coastline is less productive than any part of the Levantine basin, due to nutrient depletion in this area. This region is qualified of euphotic with low nutrient input; this is reflected on standing stocks of phytoplankton and hence on the Chl-a (Yilmaz et al., 1992).

In fact, the results of the chlorophyll-a imagery show a single winter phytoplankton bloom, peaking in February in the open water of the Levantine basin. This bloom seems to be induced by the increase of solar irradiance and the
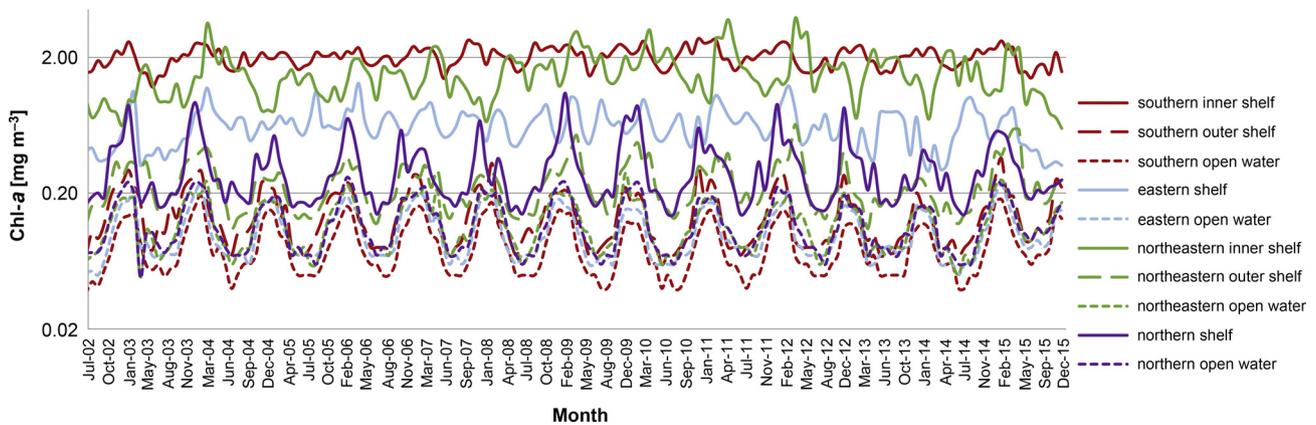
Figure 6   Monthly chlorophyll-*a* concentration averaged over the 14 studied years for each subdivided bioregion in the Levantine basin.

availability of nutrients (Krom et al., 2003). In this study, the short detected winter bloom in the open water is explained by the basin's trophic level, where the phytoplankton bloom is limited by the short nutrient availability after water mixing in winter (Krom et al., 1991, 1992). This bloom ceases shortly when the surface waters run out of nutrient. However, the spatio-temporal variability of blooms detected in our study on coastal regions is linked to the fertilization by nutrient input originating from estuaries, coastal runoffs, and anthropogenic activities, leading to an enhancement of the phytoplankton bloom.

5.2. Sea surface temperature and algal blooms

The correlation between the SST and Chl-*a* data shows a high inverse correlation factor of 0.76 while moving far from the coastal region. Fig. 8 draws an inverse Chl-*a* behavior compared to the SST. Such result can be related to several reasons such as photoacclimation, water stratification and the

optimum temperature of the blooming phytoplankton species (Xing et al., 2014). Moreover, when surface waters are cold in winter, deeper water rises to the surface bringing nutrients to sunlit areas and leading to a phytoplankton bloom.

Low correlation factors between SST and Chl-*a* recorded near the coastal area can be due to the land and anthropogenic interference. Such interference affects the annual blooming cycle *via* nutrient input originating from river runoff, as well as from urban and agricultural point sources, leading to an intensification of microbial activity coupled with the blooming of phytoplankton communities near affected areas.

5.3. Euphotic layer and algal blooms

The relationship between Chl-*a* and the attenuation coefficient seems to be strong, showing a significantly high correlation coefficient of 0.9 in all the subregions of the Levantine basin. And adding to that, the Kd_490 monthly
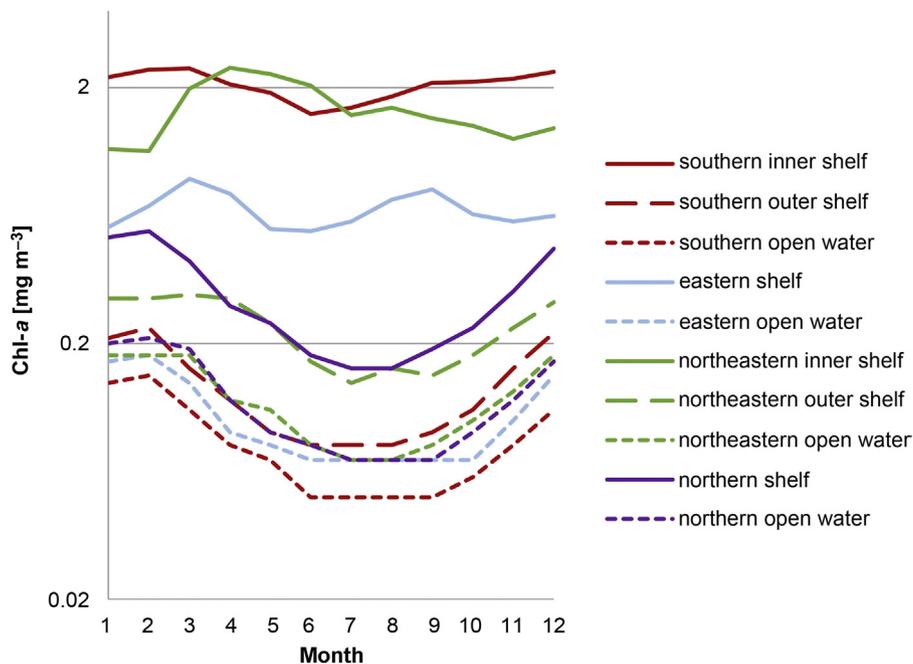

Figure 7   Monthly climatology chlorophyll-*a* concentration averaged over the 14 studied years for each subdivided bioregion in the Levantine basin.

Table 1 Descriptive statistics retrieved from the monthly images for the different biogeographic regions of the Levantine basin for the studied parameters.

Descriptive statistics			Minimum	Maximum	Mean	Std. deviation
Southern region						
	Inner shelf (<50 m)	Chl-a [mg m^{-3}]	1.40	2.75	2.06	0.31
		Kd_490 [m^{-1}]	0.12	0.20	0.16	0.02
		CDOM_index	2.44	5.38	4.25	0.54
	Outer shelf (50 m; 200 m)	Chl-a [mg m^{-3}]	0.06	0.33	0.14	0.06
		Kd_490 [m^{-1}]	0.02	0.05	0.03	0.01
		CDOM_index	2.68	5.77	3.68	0.68
	Open water (>200 m)	Chl-a [mg m^{-3}]	0.04	0.19	0.08	0.04
		Kd_490 [m^{-1}]	0.02	0.04	0.03	0.004
		CDOM_index	2.18	4.82	3.22	0.69
Eastern region						
	Shelf (<200 m)	Chl-a [mg m^{-3}]	0.29	1.29	0.67	0.18
		Kd_490 [m^{-1}]	0.04	0.11	0.07	0.012
		CDOM_index	1.60	4.71	3.39	0.59
	Open water (>200 m)	Chl-a [mg m^{-3}]	0.05	0.33	0.11	0.04
		Kd_490 [m^{-1}]	0.02	0.05	0.03	0.005
		CDOM_index	2.22	4.96	3.29	0.66
Northeastern region						
	Inner shelf (<50 m)	Chl-a [mg m^{-3}]	0.67	3.5	1.65	0.63
		Kd_490 [m^{-1}]	0.08	0.27	0.13	0.03
		CDOM_index	1.44	4.68	3.35	0.78
	Outer shelf (50 m; 200 m)	Chl-a [mg m^{-3}]	0.11	0.64	0.23	0.09
		Kd_490 [m^{-1}]	0.03	0.07	0.04	0.01
		CDOM_index	2.33	5.78	3.72	0.71
	Open water (>200 m)	Chl-a [mg m^{-3}]	0.05	0.28	0.12	0.05
		Kd_490 [m^{-1}]	0.02	0.05	0.03	0.006
		CDOM_index	2.23	5.05	3.52	0.74
Northern region						
	Shelf (<200 m)	Chl-a [mg m^{-3}]	0.14	1.09	0.31	0.18
		Kd_490 [m^{-1}]	0.03	0.1	0.05	0.015
		CDOM_index	1.3	4.81	3.18	0.86
	Open water (>200 m)	Chl-a [mg m^{-3}]	0.06	0.26	0.12	0.06
		Kd_490 [m^{-1}]	0.02	0.05	0.03	0.006
		CDOM_index	2.09	5.48	3.65	0.65

climatology in Fig. 8 shows the same pattern variability as the Chl-a in the Levantine basin, proving that the phytoplankton cycle is the first to affect the depth of the euphotic layer. In the same way, the majority of the Levantine's waters correspond to Case 1 waters.

Hotspots of turbid Case 2 waters are well indicated by the high Kd_490 and Chl-a values, noting the Nile Delta where the Nile enriches the zone with a high load of suspended materials. The Chl-a appears to be related to suspended particulate matter in high turbidity zones where the euphotic layer is
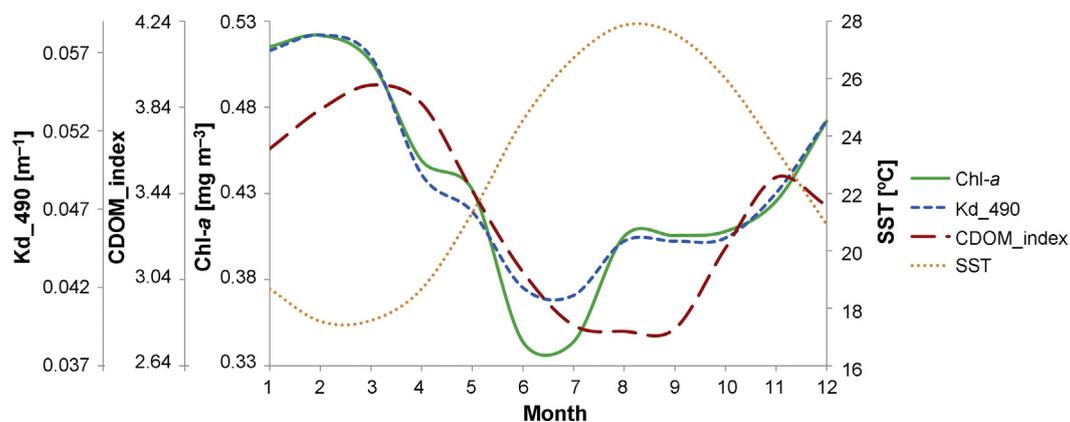
Figure 8 Chl-a, Kd_490, CDOM_index and SST monthly climatology for the Levantine basin averaged over the 14 studied years.
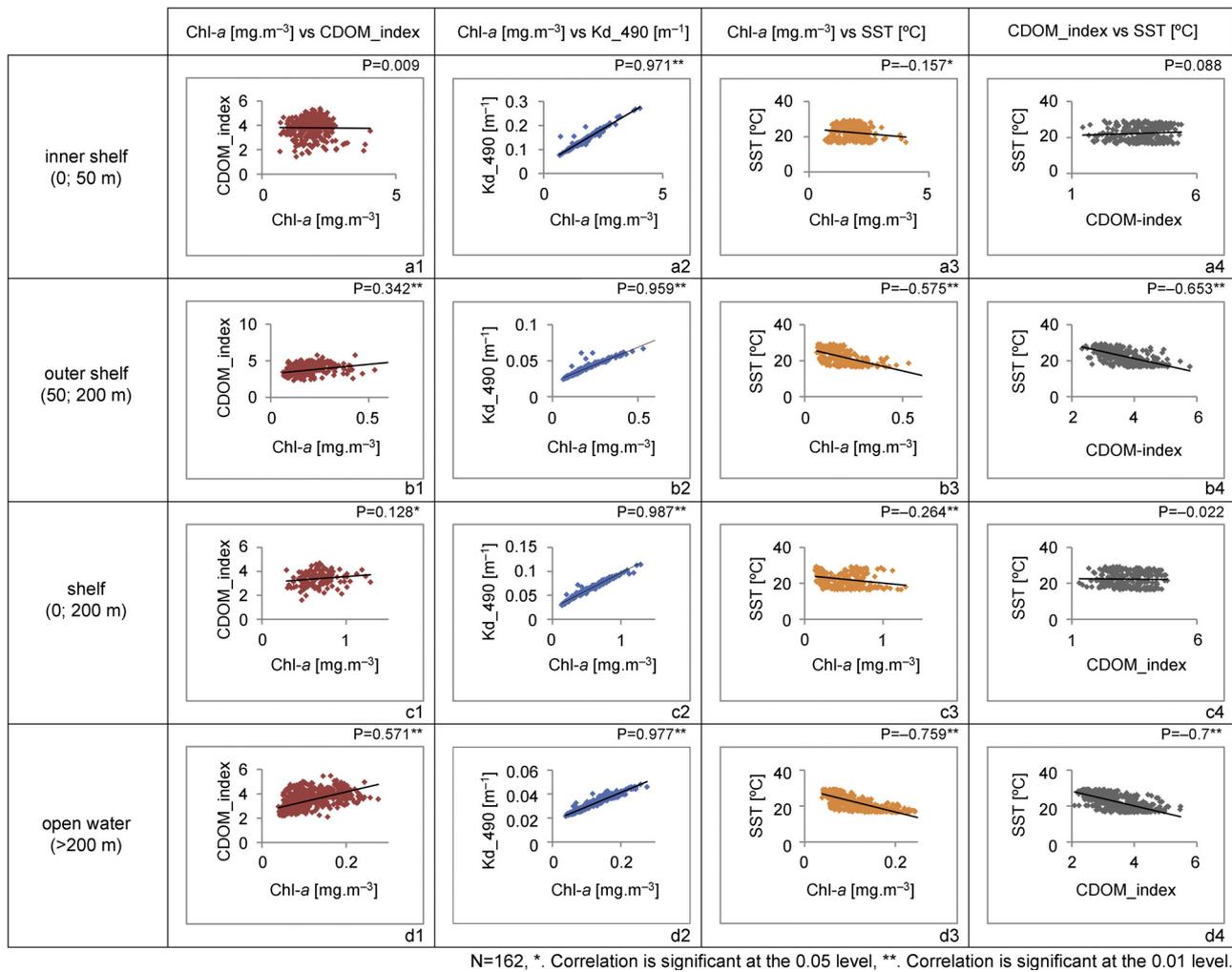
Figure 9   Scatter plots and correlation coefficients of each paired parameters in the different biogeographic regions of the Levantine basin.

shallow; algal blooms are induced by nonlimiting nutrients in very turbid water (Cloern, 1987; Harding et al., 1986; Lehman, 1992; Pennock, 1985).

5.4. Colored dissolved organic matter and algal blooms

The climatology monthly average of the Levantine basin (Fig. 8) shows a conspicuous CDOM_index peak in March, one month ahead of the Chl-*a* peak in February. The correlation coefficient between the CDOM_index and Chl-*a* in this study weakly strengthens while moving far from the coast. This can be observed also *via* the rhythmic variability gained by the averaged CDOM_index coinciding partially with the rhythmicity of Chl-*a* within the Case 1 waters. Theoretically, CDOM production is associated to the phytoplankton activity in Case 1 waters, yet many results suggested the decoupling of CDOM and phytoplankton both globally and regionally (Morel et al., 2010; Siegel et al., 2002; Xing et al., 2014). The elevation of CDOM_index to high index values can be due to the riverine runoff and point source loads in coastal regions. While in the open waters, the phytoplankton bloom activity is the principal contributor to the index variability.

The latter decrease of the CDOM_index between May and August can be mainly due to processes such as photobleaching at a high solar radiation intensity (Xing et al., 2014) and microbial activity (Coble, 2007). In fact, a high inverse correlation factor was observed in our study between the SST and CDOM_index while moving far from the coast ($\approx$0.7). This can be related to a surface CDOM depression by photobleaching processes, referred as photodegradation or photooxidation (Morel and Gentili, 2009; Xing et al., 2014), leading to say that the CDOM variability seems to be also dependent on the SST. Therefore, with the intensification of water column stratification in summer, mixing of the surface layer becomes limited by the installed thermocline; the CDOM load caught within the unmixed surface layer is exposed to high solar radiation, resulting in a significant photochemical degradation, explained by the changes in florescent properties and absorbance losses (Zhang et al., 2015). And last in September where the phytoplankton blooming starts to manifest in most of the coastal areas, the CDOM_index arises.

The CDOM_index climatology images show abnormal variability of the index in the open sea domain and highlighted by high index values (>3) with the highest values of standard deviation. As the index represents the ratio between the CDOM content and the Chl-*a*, a high index

cluster was noted at the outer shelf of the Nile, the Gulf of Iskenderun, Mersin bay and near the northern coast. These regions can be classified as a transition from Case 2 to Case 1 waters where the Chl-*a* values are quite low, yet they are in direct influence of coastal CDOM advection by surface currents. As a result, the ratio between the advected CDOM and the Chl-*a* is increased in such areas. Moreover, the variability of the CDOM and the Chl-*a* are supposedly related in the open sea, and as a result, the index should be close to 1. Such high mean values of the index in the open water bioregion indicate an overestimation of low Chl-*a* by the standard sensor algorithm while applied for the Levantine basin, referred as the most oligotrophic domain in the Mediterranean Sea. Errors in Chl-*a* estimation can be accounted to the application of standard retrieval algorithms and standard atmospheric corrections (Kowalczuk et al., 2010), which are mainly developed and validated using a global *in situ* database, reducing the specificity of the algorithm.

6. Conclusion

In this work we assessed the algal blooms in the Levantine basin, by using various optical remote sensing data from 2002 to 2015. Most of the Levantine basin's waters can be classified as Case 1 waters where the Chl-*a* and Kd_490 are co-variant, showing a strong relation between phytoplankton blooms and the determination of the euphotic depth. The CDOM and Chl-*a* were directly and indirectly related, as their relationship is mainly affected by physical and biochemical factors. The SST variability is inversely correlated to both CDOM and Chl-*a* parameters, and the CDOM variability seemed to be more related to the SST variation. In addition, phytoplankton blooms were mainly winter blooms in the open water of the Levantine basin. Spatial and temporal variability of these blooms were observed near coastal regions due to variations in the physical, biochemical and anthropogenic factors.

The data derived from MODIS imagery is a consistent source to study the temporal behavior. The overestimation of Chl-*a* values highlighted by the CDOM_index should be corrected. The problems of the lack of a proper atmospheric correction model, the availability of *in situ* data, and the complexity of the optical properties of the Levantine basin waters will remain a limitation.

References

Abboud-Abi Saab, M., 1992. Day-to-day variation in phytoplankton assemblages during spring blooming in a fixed station along the Lebanese coastline. J. Plankton Res. 14 (8), 1099—1115, http://dx.doi.org/10.1093/plankt/14.8.1099.

Abboud-Abi Saab, M., Fakhri, M., Sadek, E., Matar, N., 2008. An estimate of the environmental status of Lebanese littoral waters using nutrients and chlorophyll-*a* as indicators. Lebanese Sci. J. 9 (1), 43—60.

Abdel-Moati, M.A., 1990. Particulate organic matter in the subsurface chl-*a* maximum layer of the Southeastern Mediterranean. Oceanol. Acta 13 (3), 307—315.

Antoine, D., Morel, A., André, J.M., 1995. Algal pigment distribution and primary production in the eastern Mediterranean as derived from coastal zone color scanner observations. J. Geophys. Res. 100 (C8), 16193—16209, http://dx.doi.org/10.1029/95JC00466.

Austin, R.W., Petzold, T.J., 1981. The determination of the diffuse attenuation coefficient of sea water using the Coastal Zone Color Scanner. Oceanography from Space, vol. 13. Plenum Press, 239—256, http://dx.doi.org/10.1007/978-1-4613-3315-9_29.

Azov, Y., 1986. Seasonal patterns of phytoplankton productivity and abundance in nearshore oligotrophic waters of the Levant Basin (Mediterranean). J. Plankton Res. 8 (1), 41—53, http://dx.doi.org/10.1093/plankt/8.1.41.

Bethoux, J.P., Morin, P., Madec, C., Gentili, B., 1992. Phosphorus and nitrogen behaviour in the Mediterranean Sea. Deep Sea Res. 39 (9), 1641—1654, http://dx.doi.org/10.1016/0198-0149(92)90053-V.

Brando, V., Dekker, A., Park, Y., Schroeder, T., 2012. Adaptive semianalytical inversion of ocean colour radiometry in optically complex waters. Appl. Optics 51 (15), 2808—2833, http://dx.doi.org/10.1364/AO.51.002808.

Caddy, J.F., 1998. Issues in Mediterranean Fisheries Management: Geographical Units and Effort Control: Studies and reviews No. 70. FAO, Rome, 56 pp.

Cloern, J.E., 1987. Turbidity as a control on phytoplankton biomass and productivity in estuaries. Cont. Shelf Res. 7 (11—12), 1367—1381, http://dx.doi.org/10.1016/0278-4343(87)90042-2.

Coble, P.G., 2007. Marine optical biogeochemistry: the chemistry of ocean color. Chem. Rev. 107 (2), 402—418, http://dx.doi.org/10.1021/cr050350+.

Devlin, M., Schroeder, T., McKinna, L., Brodie, J., Brando, V., Dekker, A., 2012. Monitoring and mapping of flood plumes in the Great Barrier Reef based on in situ and remote sensing observations. In: Chang, N. (Ed.), Environmental Remote Sensing and Systems Analysis, CRC Press, Boca Raton, 147—190, (Chapter 8).

Dowidar, N.M., 1984. Phytoplankton biomass and primary productivity of the southeastern Mediterranean. Deep Sea Res. Pt. II 31 (6—8), 983—1000, http://dx.doi.org/10.1016/0198-0149(84)90052-9.

EIMP-CWMP, 2007. Annual report on status of the water quality of the Egyptian Mediterranean coastal waters during 2006. The Egyptian Environment Affair Agency, http://www.eeaa.gov.eg/eimp/reports/ArrAnualMed2006.pdf.

Harding, L.W., Meeson, B.W., Fisher, T.R., 1986. Phytoplankton production in two east coast estuaries: photosynthesis-lightfunctions and patterns of carbon assimilation in Chesapeake and Delaware bays. Estuar. Coast. Shelf Sci. 23 (6), 773—806, http://dx.doi.org/10.1016/0272-7714(86)90074-0.

Hedges, J.I., Keil, R.G., 1995. Sedimentary organic preservation: an assessment and speculative synthesis. Mar. Chem. 49 (2—3), 81—115, http://dx.doi.org/10.1016/0304-4203(95)00008-F.

Karakaya, N., Evrendilek, F., 2011. Monitoring and validating spatio-temporal dynamics of biogeochemical properties in Mersin Bay (Turkey) using Landsat ETM+. Environ. Monit. Assess. 181 (1), 457—464, http://dx.doi.org/10.1007/s10661-010-1841-5.

Kennedy, K., Schroeder, T., Shaw, M., Haynes, D., Lewis, S., Bentley, C., Paxman, C., Carter, S., Brando, V., Bartkow, M., Hearn, L., Mueller, J., 2012. Long term monitoring of photosystem II herbicides — correlation with remotely sensed freshwater extent to monitor changes in the quality of water entering the Great Barrier Reef, Australia. Mar. Pollut. Bull. 65 (4), 292—305.

Kowalczuk, P., Darecki, M., Zablocka, M., Górecka, I., 2010. Validation of empirical and semi-analytical remote sensing algorithms for estimating absorption by Coloured Dissolved Organic Matter in the Baltic Sea from SeaWiFS and MODIS imagery. Oceanologia 52 (2), 171—196, http://dx.doi.org/10.5697/oc.52-2.171.

Krom, M.D., Brenner, S., Kress, N., Neori, A., Gordon, L.I., 1992. Nutrient dynamics and new production in a warm-core eddy from the Eastern Mediterranean. Deep Sea Res. 39 (3), 467—480, http://dx.doi.org/10.1016/0198-0149(92)90083-6.

Krom, M.D., Groom, S., Zohary, T., 2003. The Eastern Mediterranean. In: Black, K.D., Shimmield, G.B. (Eds.), The Biogeochemistry of Marine Systems. Blackwell Publ., Oxford, 91—122.

Krom, M.D., Kress, N., Brenner, S., Gordon, L.I., 1991. Phosphorus limitation of primary productivity in the Eastern Mediterranean. Limnol. Oceanogr. 36 (3), 424—432, http://dx.doi.org/10.4319/lo.1991.36.3.0424.

Lavender, S.J., Moufaddal, W.M., Pradhan, Y.D., 2009. Assessment of temporal shifts of chlorophyll levels in the Egyptian Mediterranean shelf and satellite detection of the Nile bloom. Egyptian J. Aquat. Res. 35 (2), 121—135.

Lee, Z.-P., 2005. A model for the diffuse attenuation coefficient of downwelling irradiance. J. Geophys. Res. 110 (C2), http://dx.doi.org/10.1029/2004jc002275.

Lehman, P.W., 1992. Environmental factors associated with long-term changes in chlorophyll concentration in the Sacramento-San Joaquin delta and Suisun bay, California. Estuaries 15 (3), 335—348, http://dx.doi.org/10.2307/1352781.

Mann, K.H., Lazier, J.R.N., 2006. Dynamics of Marine Ecosystems: Biological—Physical Interactions in the Oceans, 3rd edn. Blackwell Publ., Malden, 496 pp.

Morel, A., Claustre, H., Gentili, B., 2010. The most oligotrophic subtropical zones of the global ocean: similarities and differences in terms of chlorophyll and yellow substance. Biogeosciences 7 (10), 3139—3151, http://dx.doi.org/10.5194/bg-7-3139-2010.

Morel, A., Gentili, B., 2009. A simple band ratio technique to quantify the colored dissolved and detrital organic material from ocean color remotely sensed data. Remote Sens. Environ. 113 (5), 998—1011, http://dx.doi.org/10.1016/j.rse.2009.01.008.

Morel, A., Huot, Y., Gentili, B., Werdell, P.J., Hooker, S.B., Franz, B.A., 2007. Examining the consistency of products derived from various ocean color sensors in open ocean (Case 1) waters in the perspective of a multi-sensor approach. Remote Sens. Environ. 111 (1), 69—88, http://dx.doi.org/10.1016/j.rse.2007.03.012.

O'Reilly, J.E., Maritorena, S., Mitchell, B.G., Siegel, D.A., Carder, K.L., Garver, S.A., Kahru, M., McClain, C.R., 1998. Ocean color chlorophyll algorithms for SeaWiFS. J. Geophys. Res. 103 (C11), 24937—24953, http://dx.doi.org/10.1029/98JC02160.

O'Reilly, J.E., Maritorena, S., O'Brien, M.C., Siegel, D.A., Toole, D., Menzies, D., Smith, R.C., Mueller, J.L., Mitchell, B.G., Kahru, M., Chavez, F.P., 2000, SeaWiFS postlaunch calibration and validation analyses, part 3, S.B. Hooker & E.R. Firestone (eds.), NASA Tech. Memo 2000-206892 Vol. 11, NASA Goddard Space Flight Center, 49 pp.

Pennock, J.R., 1985. Chlorophyll distribution in the Delaware estuary: regulation by light limitation. Estuar. Coast. Shelf Sci. 21 (5), 711—725, http://dx.doi.org/10.1016/0272-7714(85)90068-X.

Premuzic, E.T., Benkovitz, C.M., Gaffney, J.S., Walsh, J.J., 1982. The nature and distribution of organic matter in the surface sediments of world oceans and seas. Org. Geochem. 4 (2), 63—77, http://dx.doi.org/10.1016/0146-6380(82)90009-2.

Schroeder, T., Devlin, M., Brando, V.E., Dekker, A.G., Brodie, J., Clementson, L., McKinna, L., 2012. Inter-annual variability of wet season freshwater plume extent into the Great Barrier Reef lagoon based on satellite coastal ocean colour observations. Mar. Pollut. Bull. 65 (4—9), 210—223, http://dx.doi.org/10.1016/j.marpolbul.2012.02.022.

Siegel, D.A., Maritorena, S., Nelson, N.B., Hansell, D.A., Lorenzi-Kayser, M., 2002. Global distribution and dynamics of colored dissolved and detrital organic materials. J. Geophys. Res. 107 (C12), 21.1—21.14, http://dx.doi.org/10.1029/2001JC000965.

Su, J., Tian, T., Krasemann, H., Schartau, M., Wirtz, K., 2015. Response patterns of phytoplankton growth to variations in re-suspension in the German Bight revealed by daily MERIS data in 2003 and 2004. Oceanologia 57 (4), 328—341, http://dx.doi.org/10.1016/j.oceano.2015.06.001.

Tanhua, T., Hainbucher, D., Schroeder, K., Cardin, V., Álvarez, M., Civitarese, G., 2013. The Mediterranean Sea system: a review and an introduction to the special issue. Ocean Sci. 9 (5), 789—803, http://dx.doi.org/10.5194/os-9-789-2013.

Turley, C.M., Bianchi, M., Christaki, U., Conan, P., Harris, J.R.W., Psarra, S., Ruddy, G., Stutt, E.D., Tselepides, A., Van Wambeke, F., 2000. Relationship between primary producers and bacteria in an oligotrophic sea — the Mediterranean and biogeochemical implications. Mar. Ecol.-Prog. Ser. 193, 11—18, http://dx.doi.org/10.3354/meps193011.

Werdell, P.J., Bailey, S.W., 2005. An improved bio-optical data set for ocean color algorithm development and satellite data product validation. Remote Sens. Environ. 98 (1), 122—140, http://dx.doi.org/10.1016/j.rse.2005.07.001.

Xing, X., Claustre, H., Wang, H., Poteau, A., D'Ortenzio, F., 2014. Seasonal dynamics in colored dissolved organic matter in the Mediterranean Sea: patterns and drivers. Deep-Sea Res. Pt. I 83, 93—101, http://dx.doi.org/10.1016/j.dsr.2013.09.008.

Yacobi, Y.Z., Zohary, T., Kress, N., Hecht, A., Robarts, R.D., Waiser, M., Wood, A.M., Li, W.K.W., 1995. Chlorophyll distribution throughout the southeastern Mediterranean in relation to the physical structure of the water mass. J. Marine Syst. 6 (3), 179—190, http://dx.doi.org/10.1016/0924-7963(94)00028-A.

Yeh E.-N., Barnes R.A., Darzi M., Kumar L., Early E.A., Johnson B.C., Mueller J.L., Trees C.C., 1997, Case Studies for SeaWiFS Calibration and Validation, Part 4, S.B. Hooker & E.R. Firestone (eds.), NASA Tech. Memo. 104566, Vol. 41, NASA Goddard Space Flight Center, Greenbelt, Maryland, 35 pp.

Yilmaz, A., Baştürk, Ö., Saydam, A.C., Ediger, D., Yilmaz, K., Hatipoğlu, E., 1992. Eutrophication in İskenderun Bay, Northeastern Mediterranean (Science for the Total Environment). In: Vollenweider, R.A., Marchetti, R., Viviani, R. (Eds.), Marine Coastal Eutrophication. Elsevier, Amsterdam, 705—717, http://dx.doi.org/10.1016/B978-0-444-89990-3.50062-6.

Zhang, Y., Hu, C., Yu, T., 2015. Photodegradation of chromophoric dissolved organic matters in the water of Lake Dianchi, China. Front. Environ. Sci. Eng. 9 (4), 575—582, http://dx.doi.org/10.1007/s11783-014-0664-y.